

New designed helical resonator to improve measurement accuracy of magic radio frequency

Tian Guo(郭天), Peiliang Liu(刘培亮), and Chaohong Lee(李朝红)

Citation: Chin. Phys. B, 2022, 31 (**9**): 093201. DOI: 10.1088/1674-1056/ac6944
Journal homepage: http://cpb.iphy.ac.cn; http://iopscience.iop.org/cpb

What follows is a list of articles you may be interested in

Precision measurements with cold atoms and trapped ions

Qiuxin Zhang(张球新), Yirong Wang(王艺蓉), Chenhao Zhu(朱晨昊), Yuxin Wang(王玉欣), Xiang Zhang(张翔), Kuiyi Gao(高奎意), Wei Zhang(张威)
Chin. Phys. B, 2020, 29 (**9**): 093203. DOI: 10.1088/1674-1056/aba9c6

Velocity-selective spectroscopy measurements of Rydberg fine structure states in a hot vapor cell

Jun He(何军), Dongliang Pei(裴栋梁), Jieying Wang(王杰英), Junmin Wang(王军民)
Chin. Phys. B, 2017, 26 (**11**): 113202. DOI: 10.1088/1674-1056/26/11/113202

Rubidium-beam microwave clock pumped by distributed feedback diode lasers

Chang Liu(刘畅), Sheng Zhou(周晟), Yan-Hui Wang(王延辉), Shi-Min Hou(侯士敏)
Chin. Phys. B, 2017, 26 (**11**): 113201. DOI: 10.1088/1674-1056/26/11/113201

Automatic compensation of magnetic field for a rubidium space cold atom clock

Lin Li(李琳), Jingwei Ji(吉经纬), Wei Ren(任伟), Xin Zhao(赵鑫), Xiangkai Peng(彭向凯), Jingfeng Xiang(项静峰), Desheng Lü(吕德胜), Liang Liu(刘亮)
Chin. Phys. B, 2016, 25 (**7**): 073201. DOI: 10.1088/1674-1056/25/7/073201

Microwave photonic filter with a continuously tunable central frequency using an SOI high-*Q* microdisk resonator

Liu Li, Yang Ting, Dong Jian-Ji
Chin. Phys. B, 2014, 23 (**9**): 093201. DOI: 10.1088/1674-1056/23/9/093201

New designed helical resonator to improve measurement accuracy of magic radio frequency

Tian Guo(郭天)[1,2], Peiliang Liu(刘培亮)[1,2,†], and Chaohong Lee(李朝红)[1,2]

[1] *Guangdong Provincial Key Laboratory of Quantum Metrology and Sensing & School of Physics and Astronomy, Sun Yat-Sen University (Zhuhai Campus), Zhuhai* 519082, *China*

[2] *State Key Laboratory of Optoelectronic Materials and Technologies, Sun Yat-Sen University (Guangzhou Campus), Guangzhou* 510275, *China*

(Received 23 February 2022; revised manuscript received 15 April 2022; accepted manuscript online 22 April 2022)

Based upon the new designed helical resonator, the resonant radio frequency (RF) for trapping ions can be consecutively adjusted in a large range (about 12 MHz to 29 MHz) with high Q-factors (above 300). We analyze the helical resonator with a lumped element circuit model and find that the theoretical results fit well with the experimental data. With our resonator system, the resonant frequency near magic RF frequency (where the scalar Stark shift and the second-order Doppler shift due to excess micromotion cancel each other) can be continuously changed at kHz level. For $^{88}Sr^{+}$ ion, compared to earlier results, the measurement accuracy of magic RF frequency can be improved by an order of magnitude upon rough calculation, and therefore the net micromotion frequency shifts can be further reduced. Also, the differential static scalar polarizability $\Delta\alpha_0$ of clock transition can be experimentally measured more accurately.

Keywords: trapped ions, helical resonator, magic radio frequency, precision measurements

PACS: 32.30.Bv, 32.10.Dk, 37.10.Ty, 37.90.+j **DOI:** 10.1088/1674-1056/ac6944

1. Introduction

Trapped ions have been verified to be an essential tool in several fields, such as mass spectroscopy,[1–3] atomic frequency standards,[4,5] precision measurements,[6–8] quantum dynamics,[9–11] quantum information processing,[12–16] and quantum simulations.[17–20] The two most major advantages of trapped ions are long coherence time and high controllability of quantum states. Great improvements have been made with trapped ions in recent years in optical clocks,[21,22] magnetometers,[23,24] and gyroscopes.[25]

To trap ions within a radio-frequency (RF) trap, a high RF voltage is delivered to the trap electrodes to yield a deep pseudo potential well. Generally, the RF voltage is coupled to the trap with a helical resonator[26–28] which has a high Q-factor. The helical resonator is the key factor to get perfect impedance matching between the RF generator and the trap, then provides higher voltages per input power for the ion trap. On the other hand, the helical resonator has a narrow bandwidth so as to filter out the power in unwanted applied frequencies, thereby reducing their contribution to motional heating of ions.[29] Apart from the application in the RF trap, the helical resonator is also widely used in different kinds of experiments, such as for the non-destructive resonant detection of eigen-frequencies of charged particles confined in a Penning trap,[30,31] measuring the dielectric property of materials,[32] designing high frequency filter in the communication systems,[33] and applying an intense electric field for ultrasound generation.[34]

Up to now, there is still no experiment achieved a continuous change of the resonant frequency of the helical resonator in a large range and high adjusting accuracy. The main challenge is that the resonant frequency can only be changed in a very small range or discretely by altering the physical properties of the small coil of the helical resonator. However, there are many applications if the resonant frequency of the helical resonator can be adjusted in a large range with high Q-factors. For instance, we can choose an optimal trap drive frequency for longer ion confinement time. Furthermore, an accurate resonant frequency can experimentally be found to eliminate the systematic shifts caused by the micromotion-induced scalar Stark and second-order Doppler effects,[35–37] which will reduce the systematic uncertainty of optical clock.

In this paper, we present an alternative approach to continuously adjust the resonant frequency of the helical resonator in a large range. Correspondingly, the structure of the helical resonator is ingeniously designed to quickly achieve the impedance matching between the signal source and the ion trap whenever the resonant frequency is changed. In the experiment, a lumped element circuit model was developed to depict the properties of the constructed helical resonator. The resonant frequencies and Q-factors under different load conditions were measured to verify our theoretical model. Finally, we evaluate the improvement to the measurement accuracy of magic RF frequency with the experimental data.

2. Theoretical analysis

The Stark and second-order Doppler shifts induced by excess micromotion are the most important parts in the uncer-

†Corresponding author. E-mail: liupliang@mail.sysu.edu.cn

© 2022 Chinese Physical Society and IOP Publishing Ltd

tainty analysis of optical clocks. They are interrelated through the driven RF electric field. The total shift of the transition frequency due to micromotion effects can be expressed as the sum of the scalar Stark shift and the second-order Doppler shift,[35]

$$(\Delta\nu)_{\rm m} = \left[2\gamma_{\rm s}\left(\frac{M\Omega}{q}\right)^2 - \nu_0\left(\frac{1}{c}\right)^2\right]\frac{\Omega^2\sigma(1)}{(k\cos\phi)^2\sigma(0)}, \quad (1)$$

where $\gamma_{\rm s}$ is the Stark shift rate, Ω is the angular frequency of the trap field, M and q are the mass and charge of the ion, ν_0 is the transition center frequency, k is the amplitude of the wave vector of the probe light, ϕ is the angle between the observation direction and the direction of micromotion, and $\sigma(1)/\sigma(0)$ is the ratio of the first observed sideband intensity to the carrier line. According to Eq. (1), the scalar Stark and second-order Doppler shifts due to excess micromotion have the comparable magnitude but opposite signs. As a consequence, an appropriate resonant frequency can be fixed to make these two effects cancel each other, but it requires that the resonant frequency of our helical resonator can be continuously adjusted to cover the zero-crossing frequency, which is the so-called magic RF frequency.

The resonant frequency is given as $f_0 = \frac{1}{2\pi\sqrt{LC}}$. It is only related to the inductance and capacitance of the resonator system. As a result, the resonant frequency can be altered by changing the inductance or capacitance. In this work, we adopt a simple scheme for changing the resonant frequency by adjusting the variable capacitor connected in parallel with the ion trap. However, whenever the capacitance changes, the RF amplifier and its loads should be impedance matched, otherwise most of the power will be reflected back. Thus, we consider using a precision potentiometer for the first time and realize the impedance matching by adjusting it. Compared with altering the physical properties of the antenna coil[26,27] or optimizing mutual separation of two coils,[28] our method of impedance matching is simpler.

In order to evaluate the properties of the constructed helical resonator with capacitive loads, we develop a lumped element circuit model, as shown in Fig. 1. Here, Z_0 is the output impedance of the RF amplifier, $R_{\rm p}$ is the precision potentiometer, $L_{\rm a}$ is the antenna coil self inductance, $L_{\rm h}$ is the helical coil self inductance, $R_{\rm h}$ is the helical coil resistance, $R_{\rm s}$ is the shield resistance, $R_{\rm j}$ is the helical coil to shield junction resistance, $C_{\rm e}$ is the total equivalent capacitance of the resonator without load, $C_{\rm t}$ is the ion trap capacitance, R_1 is the contact resistance from the connection between the resonator and the ion trap, $C_{\rm v}$ is the variable capacitor capacitance, and R_2 is the contact resistance from the connection between the resonator and the variable capacitor. It should be noted that the capacitance of the connecting wires is not included in our model, which is negligible compared to the capacitance of the ion trap.

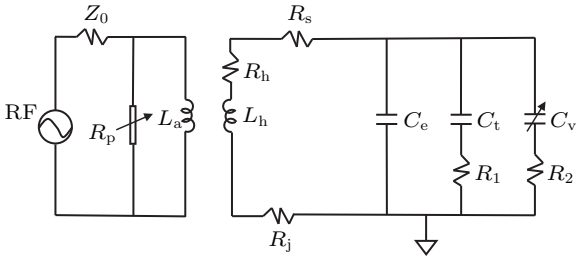


Fig. 1. Lumped element circuit model of a helical resonator with capacitive loads.

For our helical resonator system, the unloaded resonant frequency can be written as

$$f_{\rm u} = \frac{1}{2\pi\sqrt{C_{\rm e}L_{\rm h}}}. \quad (2)$$

After connecting the variable capacitor with the ion trap, the resonant frequency becomes

$$f_{\rm l} = \frac{1}{2\pi\sqrt{(C_{\rm e}+C_{\rm t}+C_{\rm v})L_{\rm h}}}. \quad (3)$$

Using Eqs. (2) and (3), we have

$$C_{\rm e} = \frac{C_{\rm t}+C_{\rm v}}{(f_{\rm u}/f_{\rm l})^2-1}, \quad (4)$$

$$L_{\rm h} = \frac{1}{4\pi^2 f_{\rm l}^2(C_{\rm e}+C_{\rm t}+C_{\rm v})}, \quad (5)$$

where $C_{\rm t}$ is a known constant. As a result, we can measure resonant frequencies for different external capacitances and then fit these data linearly to obtain the values of $C_{\rm e}$ and $L_{\rm h}$. Then the resonant frequency of the loaded resonator system can be calculated with them.

Another key parameter of helical resonator is the Q-factor. In our lumped element circuit model, the Q-factor can be expressed as

$$Q = \frac{1}{R}\sqrt{\frac{L_{\rm h}}{C_{\rm e}+C_{\rm t}+C_{\rm v}}}. \quad (6)$$

Due to helical coils with low self capacitances and low resistances, and for the loads with low resistances, R can be approximated as[27]

$$\begin{aligned} R &\approx R_{\rm h}+R_{\rm j}+R_{\rm s} \\ &\quad +{\rm Re}\left[\left(\frac{1}{\frac{-{\rm i}}{\omega C_{\rm e}}}+\frac{1}{\frac{-{\rm i}}{\omega C_{\rm t}}+R_1}+\frac{1}{\frac{-{\rm i}}{\omega C_{\rm v}}+R_2}\right)^{-1}\right] \\ &\approx R_{\rm h}+R_{\rm j}+R_{\rm s}+\frac{R_1C_{\rm t}^2+R_2C_{\rm v}^2}{(C_{\rm e}+C_{\rm t}+C_{\rm v})^2}. \end{aligned} \quad (7)$$

According to the above equations, we can estimate the corresponding resonant frequency and the Q-factor as the variable capacitor is consecutively adjusted to change the capacitance.

3. Experimental setup

Figure 2(a) shows the experimental setup to verify our theoretical analysis. The helical resonator connects to an ion trap and a variable capacitor. The variable capacitor connects in parallel with the ion trap. The internal configuration of the constructed helical resonator is shown in Fig. 2(b). The resonator system mainly consists of a copper shield, two copper coils and a precision adjustable potentiometer. The shield is a cylindrical copper tube and has two end caps of matching size. One smaller coil is called antenna coil, with which the RF amplifier connects to the helical resonator through an inductive coupling. Hence the resonator is decoupled from the resistive output impedance of the RF amplifier. The other larger coil is the helical coil, which provides a high RF voltage output for the ion trap. The precision potentiometer mounted to the top end cap is a critical component in the system. It connects in parallel with the antenna coil as shown in Fig. 2(c), and its resistance can be continuously changed from the outside of the shield.

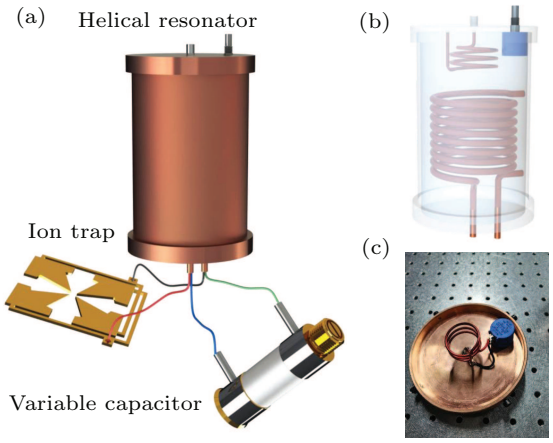


Fig. 2. (a) Experimental setup required to change the resonant frequency of the helical resonator. The helical resonator is connected to an ion trap and a variable capacitor, and the variable capacitor is connected in parallel with the ion trap. (b) Internal configuration of the helical resonator. (c) A resonator end cap showing the connection between the antenna coil and the precision potentiometer.

According to the empirical study of Macalpine and Schildknecht,[38] the helical resonator is constructed with shield diameter 114 mm, shield height 151 mm, helical coil diameter 63 mm, helical coil height 94 mm, and helical coil wire diameter 6 mm with 9 helical turns. The antenna coil is wound with 2 mm diameter copper wire. It has 3 turns of diameter 30 mm and the winding pitch is 6 mm.

4. Test results

In order to test our experimental scheme, we measure the resonant frequencies as well as the Q factors under different load conditions. The variable capacitor (Knowles Voltronics NMNT100-4) has a large adjustment range of 2–95 pF, and its capacitance can be finely changed with a slotted screwdriver. The capacitance of the ion trap is 10.5 pF measured by an LCR meter (East Tester 4510).

In the experiment, the RF signal is provided by a signal generator (Rigol DSG815). Then the signal is further amplified by an RF amplifier (Mini-Circuits ZHL-1-2W-S+). To measure the resonant frequency and Q-factor of the helical resonator, a directional coupler (Mini-Circuits ZX30-20-4-S+) is placed between the output port of the amplifier and the input port of the resonator. The reflection signal is monitored by a spectrum analyzer (Keysight N9342C) which connects to the CPL port of the directional coupler. The resonant frequency results in the minimum reflection signal detected by the spectrum analyzer. Then the reflection signal spectrum is measured by sweeping the input frequency. The resonant frequency is exactly the central frequency of the spectrum and the Q-factor is equal to the ratio of the resonant frequency to FWHM of the spectrum.

The variation of resonant frequency along with different capacitances is shown in Fig. 3. Figure 4(a) shows the linear dependence of $(C_t + C_v)$ with $(f_u/f_l)^2 - 1$. From Eq. (4), the slope of the fitting line represents the total equivalent capacitance C_e of the resonator without load, which is 6.48(2) pF. Figure 4(b) shows the linear variation of $(4\pi^2 f_l^2)^{-1}$ with $(C_e + C_t + C_v)$ and the calculated inductance L_h of the helical coil to be 1.59(1) μH. Utilizing these two values, we have calculated the resonant frequencies for different external load capacitances, as shown in the red curve in Fig. 3. It can be seen that the calculated curve is in good agreement with the experimental result and the resonant frequency is changed by about 17 MHz.

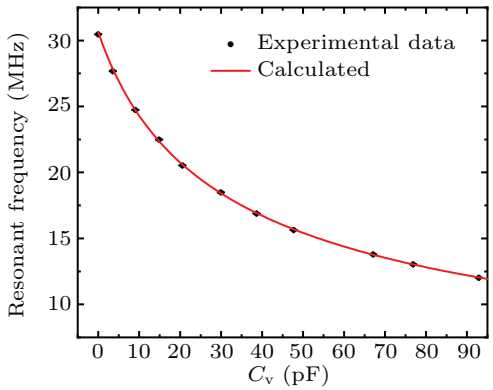


Fig. 3. Variation of resonant frequency with capacitance C_v of the variable capacitor. Each data point represents an average of four measurements, and the error bars represent one standard deviation. The red curve is the calculated result.

It should be pointed out that in other groups,[22,39] they also use variable capacitors to change the resonant frequency, but they realize the impedance matching by altering the physical properties of the antenna coil. Due to the limited ability of this method, the impedance matching cannot be well realized when the capacitance changes greatly. Therefore, the

resonant frequency can only be changed in a small range. In addition, altering the physical properties of the antenna coil will also slightly change the resonant frequency. Hence, when adjusting the variable capacitor, the resonant frequency will not change consecutively with its capacitance. However, this paper achieves the impedance matching by adjusting the precision potentiometer (BOURNS 3590S), rather than changing the internal structure of the system. As a consequence, the resonant frequency can be continuously adjustable in a large range with the resonator system in Fig. 2(a).

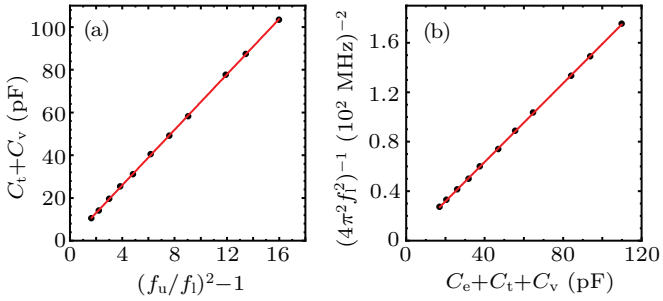


Fig. 4. (a) Linear dependence of (C_t+C_v) with $(f_u/f_l)^2-1$. (b) Linear variation of $(4\pi^2 f_l^2)^{-1}$ with $(C_e+C_t+C_v)$.

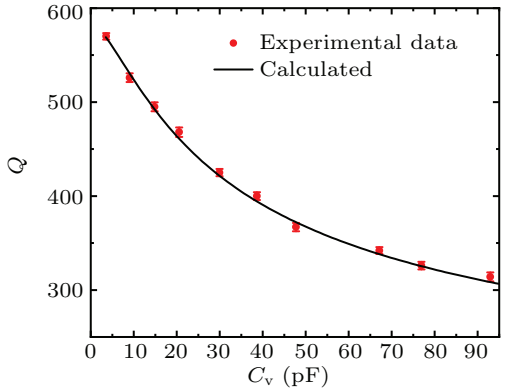


Fig. 5. Variation of Q-factor with capacitance C_v of the variable capacitor. Each data point represents an average of four measurements, and the error bars represent one standard deviation. The black curve is the calculated result.

Figure 5 shows the measurement result of Q-factor for the helical resonator. In Ref. [27], researchers showed that the resistance terms including R_h, R_j and R_s are proportional to the square root of the frequency owing to the influence of conductor skin effect. To fit the experimental result with the theoretical model, the value of $(R_h+R_j+R_s)$ is derived to be 0.600(5) Ω from Eqs. (6) and (7) by the unloaded Q-factor of 826(7) at the unloaded resonant frequency of 49.548 MHz. Thus, $(R_h+R_j+R_s)$ is $0.085(1)\sqrt{f}$ at frequency f. Since R_1 and R_2 cannot be calculated directly, we assume that they are also proportional to the square root of the frequency.[26] By applying the measured Q-factors and nonlinear least-squares-fitting of Eqs. (6) and (7), the proportional constants of R_1 and R_2 are obtained to be 0.025(6) $\Omega/(\mathrm{MHz})^{0.5}$ and 0.038(3) $\Omega/(\mathrm{MHz})^{0.5}$, respectively. With these values, the Q-factor is calculated as a function of load capacitances, shown in the black curve in Fig. 5. It is obvious that the experimental result agrees with the calculated curve well.

The long-term stability of the resonator system was also monitored, as shown in Fig. 6. Here, the resonant frequency first fixed to a certain value for some time and then was measured every half an hour within 6 h. The statistical value of the resonant frequency during the period is 14.398(2) MHz. We also changed the resonant frequency and input RF power to different values and made the same measurement. Based on the experimental data, measurement accuracy of each resonant frequency can reach kHz level and fluctuations of RF amplitude have a negligible effect on the measurement of resonant frequency. In the experiment, it can be found that the accuracy of the thousandth pF of the variable capacitor corresponds to the kHz resolution of the resonant frequency. In addition, the adjusting accuracy and stability of the variable capacitor will directly affect the resolution and stability of the resonant frequency. In Ref. [39], Dubé *et al.* proposed a method for high-accuracy measurement of the differential static scalar polarizability $\Delta\alpha_0$ by measuring the magic RF frequency Ω_0. There, they operated the test trap with frequencies between 13.5 MHz and 15.0 MHz to cover the zero-crossing frequency of 14.39(25) MHz predicted by Ref. [36], and Ω_0 was measured by comparing two $^{88}Sr^+$ ion trap systems to study the change in micromotion shifts with trap frequency. Now it is assumed that the statistical uncertainty of the trap comparison measurements is small or even ignored. With the resonator system in this paper, the resonant frequency near the zero-crossing frequency can be continuously changed at kHz level. Compared with Ref. [39], the accuracy of the fitting value of $f_0=\Omega_0/2\pi$ can be improved by at least one decimal place, so that the cancellation level of the micromotion frequency shifts can be further improved. Also, the measurement accuracy of $\Delta\alpha_0$ can be further improved. Therefore, the contribution of the blackbody radiation (BBR) frequency shift coefficient to the uncertainty of ion frequency standard can be further reduced.

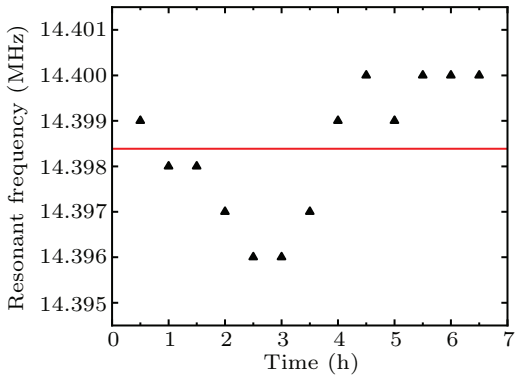


Fig. 6. Variation of resonant frequency with time. The black triangles represent the measured resonant frequencies at different times, and the red line is the average value.

5. Conclusions

In summary, we have demonstrated a helical resonator whose resonant frequency can be changed in a large range (about 12 MHz to 29 MHz) by adjusting the variable capacitor connected in parallel with the ion trap. This can be verified by treating the helical resonator with its connected loads as a lumped element circuit. Through the distinctive design, optimum impedance matching between the signal source and the ion trap can be quickly achieved by adjusting the precision potentiometer. With the resonator system presented in this paper, the resonant frequency near magic RF frequency can be continuously changed at kHz level. Compared to the results reported by Dubé *et al.*,[39] the measurement accuracy of magic RF frequency for $^{88}Sr^{+}$ ion can be improved by at least one order of magnitude, and hence the net micromotion frequency shifts can be further reduced. Promisingly, the differential static scalar polarizability $\Delta\alpha_0$ of clock transition can be experimentally measured more accurately.

Acknowledgements

Project supported by the Key-Area Research and Development Program of Guangdong Province, China (Grant No. 2019B030330001), the National Natural Science Foundation of China (Grant Nos. 12025509 and 11904418), the Science and Technology Program of Guangzhou, China (Grant No. 201904020024), and the Fundamental Research Funds for the Central Universities, China.

References

[1] March R E 1997 *J. Mass Spectrom.* **32** 351
[2] Hager J W 2002 *Rapid Commun. Mass Spectrom.* **16** 512
[3] Nolting D, Malek R and Makarov A 2019 *Mass Spectrom. Rev.* **38** 150
[4] Brewer S M, Chen J S, Hankin A M, Clements E R, Chou C W, Wineland D J, Hume D B and Leibrandt D R 2019 *Phys. Rev. Lett.* **123** 033201
[5] Huang Y, Guan H, Liu P, Bian W, Ma L, Liang K, Li T and Gao K 2016 *Phys. Rev. Lett.* **116** 013001
[6] Cairncross W B, Gresh D N, Grau M, Cossel K C, Roussy T S, Ni Y, Zhou Y, Ye J and Cornell E A 2017 *Phys. Rev. Lett.* **119** 153001
[7] Yuan W H, Deng K, Ma Z Y, Che H, Xu Z T, Liu H L, Zhang J and Lu Z H 2018 *Phys. Rev. A* **98** 052507
[8] Shao H, Huang Y, Guan H, Qian Y and Gao K 2016 *Phys. Rev. A* **94** 042507
[9] Leibfried D, Blatt R, Monroe C and Wineland D 2003 *Rev. Mod. Phys.* **75** 281
[10] Puebla R, Hwang M J, Casanova J and Plenio M B 2017 *Phys. Rev. Lett.* **118** 073001
[11] Hu C K, Santos A C, Cui J M, Huang Y F, Sarandy M S, Li C F and Guo G C 2019 *Phys. Rev. A* **99** 062320
[12] Monroe C and Kim J 2013 *Science* **339** 1164
[13] Blatt R and Wineland D 2008 *Nature* **453** 1008
[14] Steane A 1997 *Appl. Phys. B* **64** 623
[15] Zhou F, Xie Y, Xu Y Y, Huang X R and Feng M 2010 *Chin. Phys. Lett.* **27** 123203
[16] Ge W, Sawyer B C, Britton J W, Jacobs K, Bollinger J J and Foss-Feig M 2019 *Phys. Rev. Lett.* **122** 030501
[17] Lanyon B P, Hempel C, Nigg D, Müller M, Gerritsma R, Zähringer F, Schindler P, Barreiro J T, Rambach M, Kirchmair G, Hennrich M, Zoller P, Blatt R and Roos C F 2011 *Science* **334** 57
[18] Lv D, An S, Liu Z, Zhang J N, Pedernales J S, Lamata L, Solano E and Kim K 2018 *Phys. Rev. X* **8** 021027
[19] Pagano G, Hess P W, Kaplan H B, Tan W L, Richerme P, Becker P, Kyprianidis A, Zhang J, Birckelbaw E, Hernandez M R, Wu Y and Monroe C 2019 *Quantum Sci. Technol.* **4** 014004
[20] Schneider C, Porras D and Schaetz T 2012 *Rep. Prog. Phys.* **75** 024401
[21] Burt E A, Prestage J D, Tjoelker R L, Enzer D G, Kuang D, Murphy D W, Robison D E, Seubert J M, Wang R T and Ely T A 2021 *Nature* **595** 43
[22] Huang Y, Guan H, Zeng M, Tang L and Gao K 2019 *Phys. Rev. A* **99** 011401
[23] Kotler S, Akerman N, Glickman Y, Keselman A and Ozeri R 2011 *Nature* **473** 61
[24] Baumgart I, Cai J M, Retzker A, Plenio M B and Wunderlich C 2016 *Phys. Rev. Lett.* **116** 240801
[25] Campbell W C and Hamilton P 2017 *J. Phys. B: At. Mol. Opt. Phys.* **50** 064002
[26] Deng K, Sun Y L, Yuan W H, Xu Z T, Zhang J, Lu Z H and Luo J 2014 *Rev. Sci. Instrum.* **85** 104706
[27] Siverns J D, Simkins L R, Weidt S and Hensinger W K 2012 *Appl. Phys. B* **107** 921
[28] Panja S, De S, Yadav S and Gupta A S 2015 *Rev. Sci. Instrum.* **86** 056104
[29] Turchette Q A, Kielpinski D, King B E, Leibfried D, Meekhof D M, Myatt C J, Rowe M A, Sackett C A, Wood C S, Itano W M, Monroe C and Wineland D J 2000 *Phys. Rev. A* **61** 063418
[30] Nandi J, Sikdar A K, Reza A, Misra A, Das P and Ray A 2020 *Nucl. Instrum. Methods Phys. Res. A* **980** 164465
[31] Nandi J, Sikdar A K, Das P and Ray A 2022 *Rev. Sci. Instrum.* **93** 014706
[32] Deri R J 1986 *Rev. Sci. Instrum.* **57** 82
[33] Everard J K A, Cheng K K M and Dallas P A 1989 *Electron. Lett.* **25** 1648
[34] Lea M J, Tepley N and Dobbs E R 1973 *J. Phys. E: Sci. Instrum.* **6** 268
[35] Madej A A, Dubé P, Zhou Z, Bernard J E and Gertsvolf M 2012 *Phys. Rev. Lett.* **109** 203002
[36] Dubé P, Madej A A, Zhou Z and Bernard J E 2013 *Phys. Rev. A* **87** 023806
[37] Berkeland D J, Miller J D, Bergquist J C, Itano W M and Wineland D J 1998 *J. Appl. Phys.* **83** 5025
[38] Macalpine W W and Schildknecht R O 1959 *Proc. IRE* **47** 2099
[39] Dubé P, Madej A A, Tibbo M and Bernard J E 2014 *Phys. Rev. Lett.* **112** 173002